MACHINE LEARNING METHODS FOR SPECTRALLY-RESOLVED IMAGING ANALYSIS IN NEURO-ONCOLOGY

Savelieva T.A.[1,2], Romanishkin I.D.[1], Ospanov A.[2], Linkov K.G.[1], Goryajnov S.A.[3], Pavlova G.V.[3,4], Pronin I.N.[3], Loschenov V.B.[1,2]
[1]Prokhorov General Physics Institute of the Russian Academy of Sciences, Moscow, Russia
[2]National Research Nuclear University MEPhI, Moscow, Russia
[3]N.N. Burdenko National Medical Research Center of Neurosurgery, Moscow, Russia
[4]Institute of Higher Nervous Activity and Neurophysiology of the Russian Academy of Sciences, Moscow, Russia

Abstract

To reduce the frequency of relapses after surgical removal a brain tumor, it is critically important to completely remove all affected areas of the brain without disrupting the functionality of vital organs. Therefore, intraoperative differential diagnostics of micro-areas of tumor tissue with their subsequent removal or destruction is an urgent task that determines the success of the operation as a whole. Optical spectroscopy has shown its advantages over the past decade when used as a tool for intraoperative metabolic navigation. And one of the most promising options for the development of this technology is spectrally-resolved imaging. Currently, methods of spectrally-resolved imaging in diffusely reflected light have been developed, for example, mapping the degree of hemoglobin oxygen saturation, as well as fluorescence visualization systems, for both endogenous fluorophores and special fluorescent markers. These systems allow rapid analysis of tissue by the composition of chromophores and fluorophores, which allows the neurosurgeon to differentiate tumor and normal tissues, as well as functionally significant areas, during surgery. No less mandatory are the methods of using spectrally resolved visualization based on mapping characteristics obtained from Raman spectra, but due to the smaller cross-section of the process, these methods are used *ex vivo*, as a rule, for urgent analysis of fresh tissue samples. In this paper, we focus on both the physical foundations of such methods and a very important aspect of their application - machine learning (ML) methods for image processing and tissues' classification.

Keywords: optical spectroscopy, spectrally-resolved imaging, intracranial tumors, machine learning, fluorescence intraoperative navigation, fluorescence endomicroscopy, Raman microscopy, CARS, Stimulated Raman Histology, hyperspectral images.

Contacts: Savelieva T.A., e-mail: savelevat@gmail.com.

For citations: Savelieva T.A., Romanishkin I.D., Ospanov A., Linkov K.G., Goryajnov S.A., Pavlova G.V., Pronin I.N., Loschenov V.B. Machine learning methods for spectrally-resolved imaging analysis in neuro-oncology, *Biomedical Photonics*, 2024, vol. 13, no. 4, pp. 40–54. doi: 10.24931/2413–9432–2024–13–4–40–54

МЕТОДЫ МАШИННОГО ОБУЧЕНИЯ ДЛЯ АНАЛИЗА СПЕКТРАЛЬНО-РАЗРЕШЕННЫХ ИЗОБРАЖЕНИЙ В НЕЙРООНКОЛОГИИ

Т.А. Савельева[1,2], И.Д. Романишкин[1], А. Оспанов[2], К.Г. Линьков[1], С.А. Горяйнов[3], Г.В. Павлова[3,4], И.Н. Пронин[3], В.Б. Лощенов[1,2]
[1]Институт общей физики им. А.М. Прохорова Российской академии наук, Москва, Россия
[2]Национальный исследовательский ядерный университет «МИФИ», Москва, Россия
[3]НМИЦ нейрохирургии имени академика Н. Н. Бурденко, Москва, Россия
[4]Институт высшей нервной деятельности и нейрофизиологии Российской академии наук, Москва, Россия

Резюме

При проведении хирургических операций по удалению опухолей мозга критически важной для снижения частоты рецидивов является полнота удаления всех пораженных участков мозга без нарушения функциональности жизненно важных органов. Поэтому дифференциальная диагностика микроучастков опухолевой ткани с последующим их удалением или деструкцией является актуальной

задачей, определяющей успех операции в целом. Оптическая спектроскопия за последние десятилетие показала свои преимущества при использовании в качестве инструмента интраоперационной метаболической навигации. И одним из наиболее многообещающих вариантов развития этой технологии является спектрально-разрешенная визуализация. В настоящий момент разработаны методики как спектрально-разрешенной визуализации в диффузно-отраженном свете, позволяющие, например, картировать распределение сатурации гемоглобина кислородом в зоне интереса, так и системы визуализации флуоресценции, как эндогенной, так и индуцированной введением в организм пациента флуоресцентных маркеров. Эти системы обеспечивают быстрый анализ тканей по составу исследуемых хромофоров и флуорофоров, позволяя нейрохирургу во время операции дифференцировать опухолевые и нормальные ткани, а также функционально значимые зоны. Не менее важным направлением применения спектрально-разрешенной визуализации являются методы, основанные на картировании характеристик, получаемых из спектров комбинационного рассеяния, однако, в силу меньшего сечения процесса эти методики используются *ex vivo*, как правило, для срочного анализа только что удаленных образцов тканей. В настоящей работе мы сделаем фокус как на физических основаниях таких методов, так и на весьма важном аспекте их применения – методах машинного обучения для обработки таких изображений и классификации тканей.

Ключевые слова: оптическая спектроскопия, спектрально-разрешенная визуализация, внутричерепные опухоли, машинное обучение, флуоресцентная интраоперационная навигация, флуоресцентная эндомикроскопия, микроскопия комбинационного рассеяния, CARS, стимулированная Рамановская гистология, гиперспектральные изображения.

Контакты: Савельева Т.А., e-mail: e-mail: savelevat@gmail.com.

Для цитирования: Савельева Т.А., Романишкин И.Д., Оспанов А., Линьков К.Г., Горяйнов С.А., Павлова Г.В., Пронин И.Н., Лощенов В.Б. Методы машинного обучения для анализа спектрально-разрешенных изображений в нейроонкологии // Biomedical Photonics. – 2024. – Т. 13, № 4. – С. 40–54. doi: 10.24931/2413–9432–2024–13–4–40–54

Principles of formation of spectrally resolved images

Speaking about spectrally resolved imaging in biomedical applications, it is necessary to have a good understanding of what physical effects of light interaction with biological tissues lead to the formation of these images and why spectral resolution of the recorded signals is required (Fig. 1).

Light incident on a biological object can be reflected from the surface (Fresnel reflectance signal Rf) or pass through without interaction with tissue components (transmission Tc, so-called ballistic photons), but we do not consider these trivial cases in this review. From the diagnostic point of view, we are interested in those variants of light interaction with the tissue that we observe in its volume. First of all, it is necessary to keep in mind that most biological tissues are highly scattering, so light is scattered in tissues many times (this interaction is described by such an optical parameter of tissues as the scattering coefficient μ_s, which is a value inverse to the photon path length in the tissue between scattering acts). Light scattering depends on the size of scattering particles relative to the wavelength of incident light, as well as their concentration, i.e. we can judge about the structural features of tissues by this parameter. We can estimate the value of the scattering coefficient by the

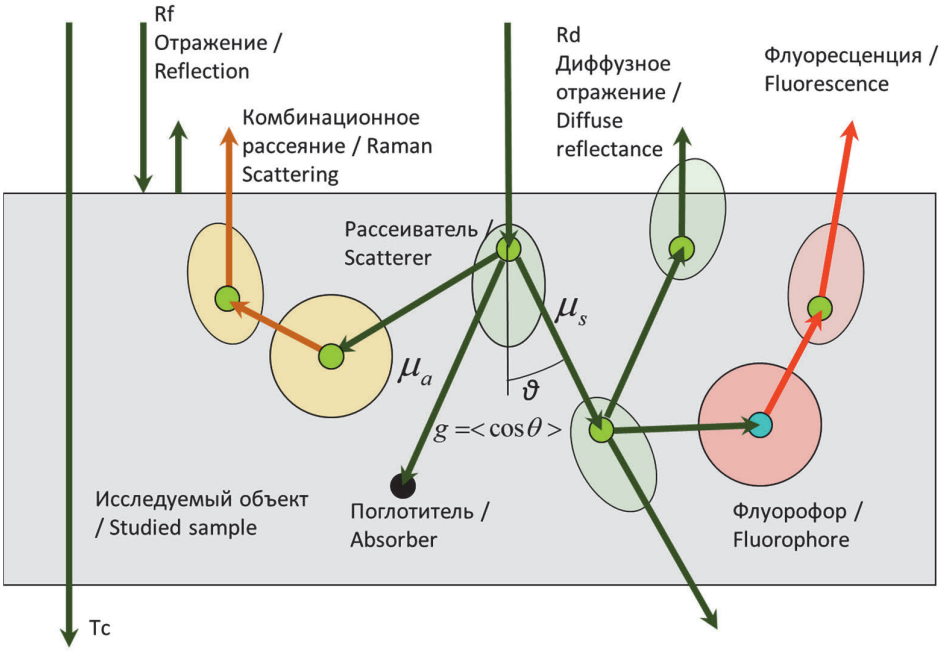

Рис. 1. Взаимодействие света с биологическими тканями.
Fig. 1. Interaction of light with biological tissues.

diffuse scattering signal (in the case of registration from the same side of the tissue from which the illumination was performed, we speak of diffuse reflectance Rd). Another important type of interaction is the absorption of light by the tissue. After light passes through the tissue, we obtain the diffuse reflectance spectrum due not only to light scattering, but also to absorption, since part of the light does not reach the receiver due to absorption, and part due to the fact that it was scattered in other directions. Therefore, from the diffuse reflectance signal, by decomposing the spectrum, it is also possible to extract the absorption spectrum of the tissue, and hence the information about the content of major absorbers, for example, hemoglobin. No less important from the diagnostic point of view is such type of interaction as fluorescence of molecules when they absorb the incident light. We distinguish between Stokes fluorescence (with energy loss due to internal relaxation) and anti-Stokes fluorescence (with energy gain), but the first variant is more probable and is much more often used in medical applications. In this case, while light scattering can occur with different probabilities at different angles (generalized scattering phase functions are indicated by colored ellipses in Fig. 1), the fluorescence signal is emitted isotropically along the direction. However, after that, the fluorescence emission also travels through the medium, scattering and absorbing repeatedly. Thus, when recording the fluorescence spectrum from biological tissues, we must remember that it has been affected by absorption and scattering and in some cases will require correction for these factors. A less probable process, but very valuable from a diagnostic point of view, is the effect of Raman scattering of light. Raman scattering is a physical process in which not only the direction of the incident light but, more importantly, the energy of the light changes as a result of the interaction. As in the case of fluorescence, we distinguish between the Stokes (energy loss) and anti-Stokes (energy gain) components of Raman scattering. Since the probability of Stokes scattering is much higher for thermodynamic reasons, we observe it most often, while the observation of the anti-Stokes component requires special technical solutions, which will be discussed below. Since the energy shift in Raman scattering is associated with vibrational sublevels of molecules, this signal allows us to estimate the molecular composition of tissues without introducing additional markers.

Spectrally resolved imaging systems can be divided into multispectral and hyperspectral imaging (MSI and HSI). Familiar examples of spectrally resolved imaging in everyday life are human color vision and the color cameras of our smartphones. The three color channels allow these systems to be classified as multispectral systems. Multispectral images typically contain between 3 and 10 bands. If more filters with narrower bandwidths are used, such a system can be called hyperspectral. Thus, the main difference between multispectral and hyperspectral images is the number of bands and their width [1].

In fact, in spectrally resolved visualization, instead of a single image, we register a hypercube of size H×W×L (frame height and width, as well as wavelength), i.e. a set of images, each of which corresponds to the brightness distribution in a certain spectral range. In this case, each spatial pixel of such an image contains information about the spectral distribution at a given point in the field of view (Fig. 2).

The two main categories of spectral imaging methods are scan-based and wide-field imaging. Point scanning (whisk-broom) methods (Fig. 3A) capture spectral data pixel by pixel. Although this method provides high spectral resolution, it requires H×W iterations to obtain a hypercube, which is time-consuming for megapixel images and limits their use for capturing static scenes and/or small fields of view. Linear scanning (push-broom) methods (Fig. 3B) use a linear detector oriented perpendicular to the scanning direction (e.g., row detec-

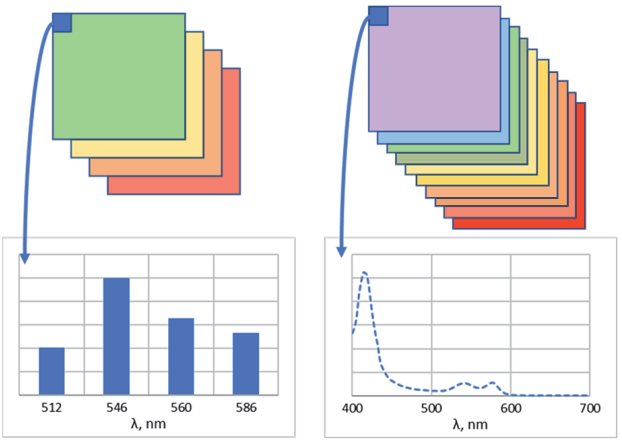

Рис. 2. Различие мультиспектральных и гиперспектральных изображений.
Fig. 2. Difference between multispectral and hyperspectral images.

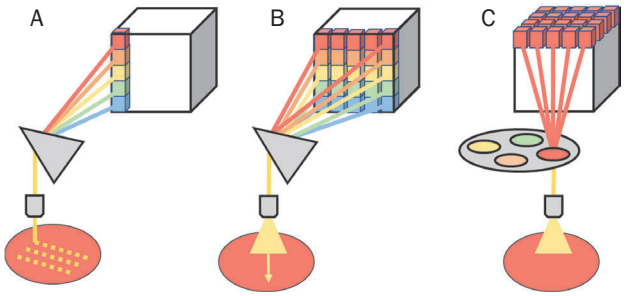

Рис. 3. Различные методы получения гиперспектральных данных (A – точечное сканирование, B – линейное сканирование, C – спектральное сканирование).
Fig. 3. Different methods of obtaining hyperspectral data (A – point scanning, B – line scanning, C – spectral scanning).

tors scan along columns), and spectral data are collected row by row. This approach reduces the number of registrations to the number of rows or columns in the image, which significantly decreases the registration time compared to point scanners. These are the most common systems that are widely used in HSI applications [2].

Wide-field imaging is a method of simultaneously illuminating and, consequently, detecting the entire field of view in an array of points (pixels of the detector array). Compared to scan-based imaging methods, wide-field imaging eliminates the need for mechanical scanning and allows a large area to be imaged in a single scan.

Spectral scanning methods (Fig. 3C) are essentially related to wide-field imaging as they allow one spectral channel in a hyperspectral cube to be imaged at a time. For this purpose, it is possible to use a tunable bandpass spectral filter for sequential acquisition of two-dimensional images in each spectral channel. It is possible to implement this principle through filters at the receiver, as well as time multiplexing of light sources, for example. Snapshot methods provide a hyperspectral cube with full spatial and spectral information in a single exposure. Snapshot acquisition is achieved by multiplexing the sensor with spatial separation in spatial and spectral dimensions. It can be several cameras separated by beam splitters, mosaically arranged filters on the detector matrix or separation of the detector matrix into macro zones for different filters.

Video fluorescent systems

At the end of the 20th century, W. Stummer [3] presented the results of the study of fluorescence of 5-ALA-induced protoporphyrin IX (Pp IX) in patients with glioblastoma, which initiated a new round of interest in fluorescence in surgical practice. Pp IX is not injected itself, but accumulates in tumor tissues as a product of the metabolism of 5-aminolevulinic acid, which is used as a drug for administration. This determines a number of its interesting properties as a tumor marker [4–6]. Another porphyrin-based fluorescent tumor marker chlorin e6 is promising for application in neuro-oncology [7]. Since then, the use of Pp IX and chlorin e6 has become widespread in neurosurgery [8, 9] and has gone beyond an exclusively spectroscopic technique – in many neurosurgical clinics and departments, fluorescence video navigation is a routine part of brain and spinal cord tumor removal [10].

Fluorescence is the emission of light by an atom or molecule in an electronically excited state (in particular, due to light absorption) (Fig. 4). Fluorescence is one variant of the radiative relaxation of a molecule from an excited state.

Video systems for fluorescence navigation in neurosurgery can currently be divided into wide field of view and microscopic systems.

The principle of working of systems with a wide field of view is to illuminate the entire area of interest with a light source, the wavelength of which coincides with one of the maxima in the absorption spectrum of the detected fluorescent markers. For example, protoporphyrin IX, which is widely used in neurosurgery, has a strong absorption band in the violet region, the so-called Soret band, as well as a Q-band of absorption closer to the window of biological transparency, therefore, light sources with wavelengths coinciding with all local absorption maxima of this molecule can be used for its excitation. For fluorescence detection a cross filter system is necessary: an illuminating filter suppressing the excitation light in the spectral range of fluorescence registration, and an imaging filter installed before the photodetector suppressing the excitation light, which is necessary because fluorescence is several orders of magnitude lower in intensity than the light that excites it.

Among the systems with a wide field of view, the Opmi Pentero Carl Zeiss microscope with Blue 400 mode, which allows to observe fluorescence of Pp IX when excited by violet light, is actively used in neurosurgical practice. The main limitation of using this mode is the presence of blood in the wound, which absorbs visible light in the short-wave region, preventing it from penetrating deeper – to the tissues under study. This limitation can be avoided by using an excitation source not in the short-wave range of the spectrum, in which most of the biological molecules absorb light, but, for example, in the first window of biological transparency in the red region, as it was proposed in [11]. The authors created an endoscopic system for visualizing the distribution of

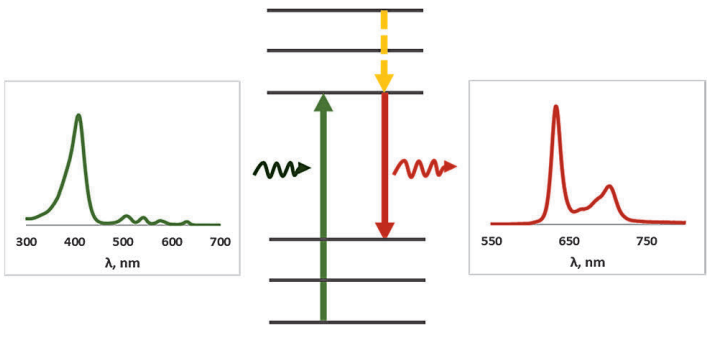

Рис. 4. Диаграмма Яблонского с энергетическими переходами, иллюстрирующими принцип поглощения света молекулой и испускания флуоресценции в стоксовой области.
Fig. 4. Jablonski diagram with energy transitions illustrating the principle of light absorption by a molecule and fluorescence emission in the Stokes region.

Pp IX that combines full-color and fluorescence imaging and calculates the concentration of the photosensitizer under study in the central region. A system combining a neurosurgical aspirator and the technique of fiber-optic spectroscopy and spectrally resolved endoscopy during surgeries for brain tumor removal was also based on this technical solution [12]. In this implementation, a fixed distance from the endoscope end face to the tissue allows calibrating the system by fluorescence level and quantifying the fluorophore concentration in the tissue by signal brightness. Research is also underway on the use of photo and spectral fluorescence analysis of the area of spinal cord injury [13] or tumors [14].

In [15], a spectrally resolved video fluorescence system integrated into a commercial neurosurgical microscope is presented that allows quantitative estimation of Pp IX content by correcting the effects of optical absorption and tissue scattering in the detected fluorescence signal.

Despite the fact that the best delineation of tumor tissues by fluorescent dye can be observed in high-grade tumors, a large amount of work is also devoted to fluorescence navigation in the removal of intracranial low-grade tumors [16].

Intraoperative microscopy (microscopic imaging with cellular and subcellular spatial resolution and millimeter field of view) is also used as a tool for intraoperative surgical navigation in brain tumor resection. Confocal microscopy or confocal laser endomicroscopy (CLE) [17] using portable probes provide *in vivo* registration of microstructural images, allowing intraoperative visualization of structures at depth, in three dimensions, with histological detail (depending on the fluorescent markers used). It is based on the principle of optical scanning by laser beam of the entire field of view and registration of fluorescent emission through small apertures (pinholes) placed in the path of light for selective display of photons from a certain focal plane.

The first results of using the Optiscan FIVE 1 fiber-optic confocal system (Optiscan Pty Ltd, Australia) for neurosurgery were published in [18] in 2010. This device contains a miniature fiber-optic probe, excitation and fluorescence radiation are transmitted through a single fiber. The system provides non-invasive image registration by optical sectioning at a known depth. The system has been validated in C57/BL6 laboratory animals with GL26 glioblastoma. Fluorescein (0.1% Pharmalab, Australia) and acriflavine (0.05% Sigma Chemicals, Australia) were used as fluorescent dyes. Another example of using the Optiscan system on animals with C6 glioma and fluorescein as a dye was published in [19]. In addition to fluorescein, the authors also used acriavin, indocyanine green and fluorescein isothiocyanate as dyes. Their results allowed morphological analysis and correlated well with classical histological images of the same tumor sections. Another work using the Optiscan intraoperative confocal microscopy system was performed by Martirosyan et al. on animals with C6 gliomas and indocyanine green as a fluorescent marker [20].

A study of the method of confocal laser endomicroscopy with fluorescein was conducted in clinical conditions on a sample of 33 patients with brain tumors [21]. A definite breakthrough in this direction was the study [22] conducted in clinical conditions on patients with benign glial tumors using Pp IX as a fluorescent marker; at the same time, due to the peculiarities of the drug accumulation in cells, it was not a question of morphological analysis, as it was demonstrated in the works with fluorescein. The differences between tumor and normal tissue were determined by the number of luminous cells in the field of view. However, even in this case, it is possible to detect some correlation between the intraoperative picture and the histologic picture obtained in the laboratory. The work [23] was also performed in clinical conditions using the same endomicroscope, but fluorescein administered intravenously immediately before the endomicroscope analysis procedure was used as a marker. The results obtained correlated well with data from classical pathomorphology. A distinctive feature of this work is the rather broad coverage of different types of intracranial tumors. Various artifacts of the intraoperative confocal system, particularly shear artifacts and blood shielding of the signal, are also discussed in this paper.

In [24], two contrast agents, fluorescein and 5-ALA induced protoporphyrin IX with excitation in the blue range of the spectrum, were used for confocal laser endomicroscopy (Cellvisio system, Maune Kea Technologies, Paris, France). This device uses a fiber optic bundle as a sensor, in which each fiber functions as a pinhole. One disadvantage of this device is the inability to adjust the depth of focus, and another is the autofluorescence of the fiber material when excited at 405 nm, making it difficult to use for excitation of 5-ALA Pp IX in the Soret band [25]. The study was performed on a sample of 9 patients, of which 6 had open surgery and 3 had stereotactic biopsy.

Summarizing the features of confocal laser endomicroscopy systems, it can be seen that structural analysis close to classical pathomorphology is achieved using fluorescein. In this case, fluorescein is predominantly an extracellular contrast agent, penetrating only through the disrupted blood-brain barrier. When malignant gliomas are observed, it provides an intense fluorescent background. Cells and intracellular structures are identified as transparent or darker structures on the fluorescent background. Erythrocytes are visualized against the background in the same way. If the distal end of the probe is not cleaned, artifacts from blood can reduce image quality and affect the analysis. These

disadvantages suggest the advantages of using dyes that are excitable and fluorescent in the red and near-infrared, such as Pp IX and indocyanine green. Pp IX is a more tumor-specific dye.

The main obstacle to the widespread use of laser confocal scanning microscopy in intraoperative analysis is the scanning principle itself. Sufficiently long scanning time (on average about 1 second for 1 frame for different systems) leads to the appearance of shear artifacts and to a decrease in the decoding properties of the obtained images. A system combining a spectrally resolved quantitative imaging device with a wide field of view and a fluorescence endomicroscope is described in [26]. Spectral resolution is achieved by using a tunable liquid crystal filter with a half-width of 20 nm in the range of 400–720 nm. The system already mentioned above, Cellvizio (Mauna Kea Technologies), is used as a fluorescence endomicroscope. In [27], it was shown that over a wide range of fluorophore concentrations, the ability of a video system using red light to excite fluorescence at different depths along the image axis up to 6 mm below the surface allows resolution of multiple fluorescent foci at a distance of 2 mm in the same plane or at different depths along the image axis at a distance of 3 mm. Second-generation CLE systems, such as the ZEISS CONVIVO (Carl Zeiss Meditec AG, Oberkochen, Germany), have been specifically designed for neurosurgical use and have undergone a number of clinical trials in recent years. CONVIVO has been used in animal models and in *ex vivo* and *in vivo* experiments, confirming its feasibility with fluorescein as a technology capable of providing real-time *in vivo* histopathologic data [28–31].

Hyperspectral imaging in diffuse-reflected light

Biological tissues are mostly strongly scattering media, i.e. light falling on them is multiply scattered by fluctuations of the refractive index in the medium. Part of the light returns to the detector, forming the so-called diffuse reflectance (DR) signal (Rd on Fig. 1). Since light is not only scattered in tissues, but part of it is also absorbed by tissue chromophores, the detected spectrum carries information about both scattering and absorbing properties of tissues. The main chromophore in the visible part of the spectrum is hemoglobin. Due to differences in the absorption spectrum of hemoglobin in oxygenated and reduced forms, it is also possible to estimate the local level of hemoglobin oxygen saturation using DR spectra.

The work [32] is devoted to the analysis of fresh *ex vivo* glioma samples using both a laboratory spectrophotometer and a hyperspectral system, which is based on spectral scanning of samples using illumination by a supercontinuum laser (SCL) filtered by acousto-optic tunable filters (AOTF). When comparing spectrophotometry and hyperspectral imaging data, significant differences were found between individual regions in two spectral ranges: between 510 and 660 nm (which can be attributed to variations in hemoglobin concentration and oxygenation) and between 780 and 880 nm (which can be either hemoglobin or cytochrome c oxidase).

The HELICoiD system is presented in [33, 34]. It consists of two hyperspectral cameras. The first one operates in the visible and near-infrared spectral range (400–1000 nm), and the second one operates in the near-infrared range (900–1700 nm). These cameras are connected to a scanning device with a push rod. The illumination system provides cold light from 400 to 2200 nm through an optical fiber connected to a quartz tungsten-halogen lamp. The hyperspectral system is based on the line-scanning method and provides a spectral resolution of 2–3 nm, allowing identification of tumor tissue and vascular structures. In [35], the authors performed a statistical analysis of hyperspectral images of brain tumor patients from the HELICoiD dataset to identify correlations between reflectance and absorption spectra of tissue chromophores, also finding a correlation with cytochrome. The authors of [36] showed that the spectral bands 440.5–465.96 nm, 498.71–509.62 nm, 556.91–575.1 nm, 593.29–615.12 nm, 636.94–666.05 nm, 698.79–731.53 nm, and 884.32–902.51 nm are the most relevant for classification of brain tumor tissues based on hyperspectral images.

Raman scattering-based visualization

One of the most actively developing areas of spectral analysis in neuro-oncology at present is Raman spectroscopy [37–39]. As mentioned above, Raman scattering not only changes the direction of the incident radiation, but the probability of this process is lower than in the case of elastic scattering, and both an increase in energy (anti-Stokes component) and a decrease (Stokes component) are possible (Fig. 5).

Raman spectroscopy has many applications in medicine due to its ability to characterize individual molecules and biological tissues. Characteristic shifts in the Raman spectrum correspond to specific vibrational modes of chemical bonds. For example, the symmetric stretching mode of -CH_2 plays an important role in the characterization of biomedical samples, allowing the detection of fatty acids [40].

Three characteristic spectral bands in the Raman spectrum were used in [41] to create a virtual RGB color scheme. Red (1004 cm^{-1} channel corresponding to phenylalanine), green (1300–1344 cm^{-1}, CH deformations in protein and collagen) and blue (1600 cm^{-1}, C=O and C=C of the 1st amide band, lipids and nucleic acids) color scales encoded the intensities in the corresponding Raman spectral bands. On such color maps it was possible to distinguish white matter, gray matter, and tumor tissue with a diagnostic accuracy of about 90%.

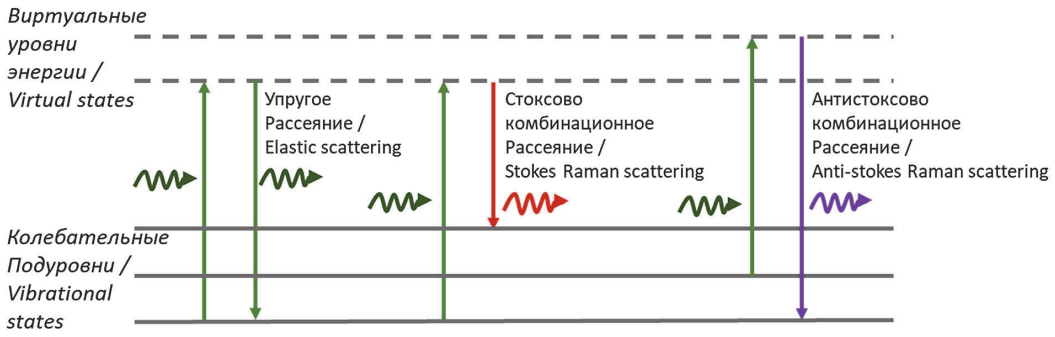

Рис. 5. Диаграммы Яблонского, иллюстрирующие эффект комбинационного рассеяния и его отличие от упругого рассеяния.
Fig. 5. Yablonsky diagrams illustrating the effect of Raman scattering and its difference from elastic scattering.

Spontaneous Raman scattering is the most accessible method in terms of cost, but due to the low cross section of the process the signal is too weak and exposure times on the order of several minutes are required. A number of approaches improve the sensitivity of the process. Instead of obtaining broadband Raman spectra in the range (0–3500 cm^{-1}), coherent Raman microscopy methods increase the signal intensity by targeting a specific wave number using a second excitation laser beam to coherently control the vibrational frequency of the active chemical Raman bonds. The two main techniques using this approach and applied to brain tumor imaging are stimulated Raman histology (SRH) and coherent anti-Stokes Raman scattering (CARS) microscopy.

A series of works [42, 43] presents the results of the application of a spectrally-resolved Raman based visualization technique for the analysis of images structurally similar to histological hematoxylin-eosin (H&E) images, but obtained using stimulated Raman scattering with a dual-wavelength fiber laser with a fixed pump wavelength of 790 nm and Stokes wavelengths in the range from 1015 nm to 1050 nm. For Stimulated Raman Histology (SRH) study, samples were sequentially scanned at two Raman shifts: 2850 cm^{-1} and 2950 cm^{-1}. Lipid-rich brain regions (e.g., myelinated white matter) show high signal at 2845 cm^{-1} due to symmetric CH_2 stretching in fatty acids. Cellular regions show high intensity at 2930 cm^{-1} and high S_{2930}/S_{2845} ratio, indicating high protein and DNA content. The resulting maps of the intensity ratios at these two peaks were converted to pseudocolor using the H&E coloring scheme. Convolutional neural networks (CNN) were used to classify the resulting images. This is a very promising method to use the entire array of currently accumulated H&E histologic slices as a training sample.

In work [44], CARS microscopy was used to visualize fresh unfixed and unstained *ex vivo* specimens from a mouse model of orthotopic human astrocytoma. The histologic features shown on CARS images were comparable to standard H&E histology. Chemically selective images of lipids (2845 cm^{-1}, symmetric CH_2 stretching) and proteins (CH_3 stretching, 2920 cm^{-1}; amide I band, 2960 cm^{-1}) allowed the delineation of the brain tumor boundary in a mouse model. The authors [45] used molecular C-H vibrations in different cryosectioned brain tumors (glioblastoma, melanoma, and breast cancer metastases) to assess lipid content compared to normal brain tissue, demonstrating that all tumor types have lower CARS lipid signal intensity than normal parenchyma.

Methodology for the application of machine learning in analyzing spectrally resolved images

Machine learning (ML) methods are used for spectrally resolved images at several levels. First, for image processing and segmentation, and second, for data classification. The combination of these methods is usually combined by the term machine vision. However, in the case of spectrally resolved images, we have a hypercube of data, i.e. the dimensionality we operate on is higher than when analyzing conventional images. At the same time, the sampling volume, as is often the case in medical applications, is limited by the image registration procedure itself.

Typically, to develop effective clinical decisions, AI models are trained to reproduce expert performance on large amounts of well-annotated data, leading to reasonably accurate and reproducible results in medical image analysis. However, this approach is critically dependent on the availability of large annotated datasets. Strict regulatory restrictions on medical data sharing and the opportunity cost for physicians to annotate data make the generation of large datasets far from a trivial task [46] Several approaches have been used to increase the amount of available data, such as synthetic dataset generation [47] or artificial expansion of available annotated datasets [48]. More non-trivial approaches are also possible, as in the case of histology based on Raman spectroscopy, where two characteristic peaks for proteins and lipids allow the generation of a pseudo-color image that mimics histological tissue images when stained with hematoxylin-eosin, which immediately opens access to huge databases of pathomorphological data [49]. The method of laser confocal endomicroscopy with

fluorescein offers a similar expansion of the annotated data base.

The stage of preprocessing of recorded signals is critical for successful tissue classification using spectrally resolved data, including images. In works devoted to hyperspectral imaging systems, a general algorithm can be identified, including such stages as formation of the hypercube of data (regardless of the type of scanning used), background correction, correction on the white and dark reference images, spectral correction, normalization, and often a synthetic full-color image. When analyzing spectrally resolved images based on the Raman effect, the algorithm includes removal of "silent" regions in the spectrum (those that do not contain characteristic peaks), cosmic rays removal, baseline and fluorescence correction, normalization.

Hyperspectral imaging has shown remarkable results as a diagnostic tool for tumor detection in various medical applications. In [50], using a k-fold cross-validation approach, they demonstrated that HSI combined with the proposed processing system (Table 1) is a promising intraoperative tool for in-vivo identification and delineation of brain tumors, including both primary (high and low malignancy) and secondary tumors. The obtained data were transformed into a set of spectral and spatial features with subsequent classification using both classical machine learning and deep learning methods [51].

An important stage of work with spectral data is the choice of a dimensionality reduction method. Among the most commonly used methods are feature filtering methods based either on a priori data on biochemical composition of tissues or on the results of statistical analysis and selection of those features that provide statistically significant differences between classes of data. Another widely used approach is the use of feature projection methods, among which the principal component analysis (PCA) is the most popular. PCA is used to project a higher-dimensional data matrix onto a low-component subspace. It reduces the set of variables to a smaller set of orthogonal, and thus independent, principal components in the direction of maximum variation, i.e., it reduces the dimensionality and preserves the most significant information for further analysis. Linear discriminant analysis (LDA) and, somewhat less frequently, quadratic discriminant analysis (QDA) are also frequently used for this purpose. The main goal of linear discriminant analysis (also called Fisher's linear discriminant) is to find "axes of discrimination" that optimally classify data into two or more classes. LDA is closely related to PCA (Principal Component Analysis) in that both look for latent axes that compactly explain the variance in the data. The main difference between PCA and LDA is that LDA is a supervised method and PCA is an unsupervised method. PCA looks for predictions that maximize the variance, and LDA looks for predictions that maximize the ratio of interclass variance to intraclass variance. QDA is a classifier with a quadratic decision boundary, generated by fitting class conditional densities to the data and using Bayes' rule.

Another way to reduce the dimensionality of the data is the t-Distributed Stochastic Neighbor embedding (t-SNE) algorithm. It is a nonlinear dimensionality reduction method well suited for embedding high-dimensional data for visualization into a low-dimensional space of two or three dimensions. In the higher dimension space, a probability distribution over pairs of points is constructed in such a way that similar points are assigned a high probability, and dissimilar points are assigned a lower probability. And in the lower dimension space, the algorithm tries to achieve similar probability distribution by minimizing Kullback–Leibler divergence between two distributions. t-SNE tries to preserve the relative positions of points in lower dimensional mapping.

To deal with high-dimensional hyperspectral data, a dimensionality reduction method with manifold embedding can also be used. This method uses a modified version of t-SNE based on deep learning, called t-SNE with fixed references (FR-t-SNE). This nonlinear embedding method seeks to preserve local spatial regularity (nearby pixels have a high probability of representing the same class) while preserving high-level global features (pixel classes) [52].

Both classical machine learning methods such as support vector machine (SVM) method, linear and quadratic discriminant analysis, ensembles of random forest (RF) based algorithms, and methods based on neural networks are used to classify tissues according to the

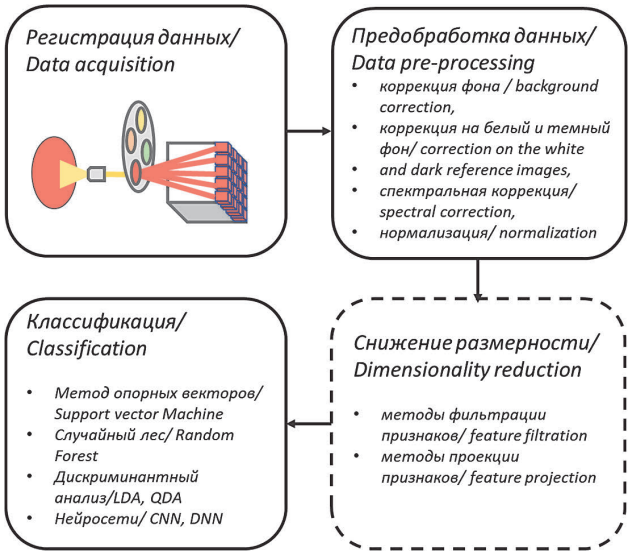

Рис. 6. Блок-схема основных этапов анализа спектрально-разрешенных изображений.
Fig. 6. Flowchart of the key steps involved in the analysis of spectrally-resolved images.

obtained features (Table 1). SVM method is a supervised machine learning algorithm that predicts an optimal hyperplane in n-dimensional space to divide the training set into several classes. Depending on the problem, different kernel functions can be defined for the decision function to add another dimensionality to the data, allowing better partitioning into classes. The algorithm proposed in the study [53] used a hybrid approach that combined both supervised and unsupervised machine learning methods. First, supervised pixel classification using SVM was performed. The generated classification map was spatially homogenized using the t-SNE dimensionality reduction algorithm and K-nearest neighbor (KNN) filtering. The information obtained from the supervised stage was merged with the segmentation map obtained by clustering. The merging was performed using a majority voting approach that associates each cluster with a particular class.

A combined approach was also used in [54]. The KNN-based filtering algorithm receives an input image that consists of probability maps estimated by the SVM classifier and a hypercube representation at one of the wavelengths generated using a dimensionality reduction algorithm such as PCA. The result is a classification map where each pixel is assigned to the most likely class. The nearest neighbors of a particular pixel are searched in the feature space, which contains both the pixel value and spatial coordinates.

Таблица 1.
Методология, используемая при классификации спектрально-разрешенных изображений, регистрируемых в условиях *in vivo*

Table 1.
Methodology used in the classification of spectrally resolved images recorded *in vivo*

Источник Source	Тип сигнала Signal type	Снижение размерности Dimensionality reduction	Методы МО ML methods
Ayaz 2022 [57]	ГСВ (ЛС) HSI (push-broom)	Автокорреляции и инкрементальный МГК The autocorrelation and incremental PCA	3D CNN
Baig 2021 [58]	ГСВ (ЛС) HSI (push-broom)	Эмпирическая модовая декомпозиция, выбор признаков EMD (Empirical Mode Decomposition), feature selection	SVM
Cruz-Guerrero, 2020 [59]	ГСВ (ЛС) HSI (push-broom)	Расширенное слепое извлечение конечных элементов и распространенности Extended blind end-member and abundance extraction (EBEAE)	Слепое линейное разложение Blind linear unmixing, SVM
Ezhov, 2023 [35]	ГСВ (ЛС) HSI (push-broom)	МГК PCA	
Fabelo, 2016 [33]	ГСВ (ЛС) HSI (push-broom)		SVM, CNN, RF
Fabelo, 2018 [53]	ГСВ (ЛС) HSI (push-broom)	t-SNE	SVM, KNN
Fabelo, 2019 [51]	ГСВ (ЛС) HSI (push-broom)	Эмпирический выбор трёх спектральных каналов Empirical choice of three spectral channels	2D-CNN, DNN
Florimbi, 2018 [54]	ГСВ (ЛС) HSI (push-broom)	PCA	SVM, KNN
Leon, 2023 [50]	ГСВ HSI	PCA	SVM, RF, KNN, DNN
Ravi, 2017 [52]	ГСВ (снимок) HSI (Snapshot)	Вложение многообразий Manifold embedding	STF
Ruiz, 2020 [60]	ГСВ (снимок) HSI (Snapshot)		SVM, RF
Salvador, 2016 [61]	ГСВ (ЛС) HSI (push-broom)		SVM, RF, CNN, KKN
Sutradhar, 2022 [62]	ГСВ (снимок) HSI (Snapshot)		SVM
Torti, 2018 [63]	ГСВ (ЛС) HSI (push-broom)	PCA	SVM, KNN
Urbanos, 2021 [64]	ГСВ (снимок) HSI (Snapshot)		SVM, RF и CNN

*ГСВ – гиперспектральная визуализация, ЛС – линейное сканирование, МГК – метод главных компонент, ЛДА – линейный дискриминантный анализ, КДА – квадратичный дискриминантный анализ, SVM – метод опорных векторов, RF – случайный лес, KNN – метод k ближайших соседей, CNN – конволюционная нейросеть, DNN – глубокая нейросеть, STF – семантический текстовый лес
*HSI – Hyperspectral Imaging, PCA – Principal Component Analysis, LDA – linear discrimimnant analysis, QDA – Quadratic Discriminant Analysis, SVM – Support Vector Machine, RF – Random Forest, KNN – k Nearest Neighbors, CNN – Convolutional Neural Network, DNN – Deep Neural Network, STF – Semantic Texton Forest

A random forest (RF) is an ensemble-based machine learning algorithm with a teacher that uses decision trees as a base. For classification tasks, the output of a random forest is the class selected by the majority of trees. For regression tasks, the output is the average of the predictions of the trees. Studies on the use of RF [55, 56] have proved that it is a successful classifier when hyperspectral images are used.

Convolutional neural networks (CNNs) have an advantage over classical machine learning methods in that they actually implement both stages: feature extraction and classification. In the feature extraction block, convolutions are performed to detect patterns in spatial and spectral dimensions, resulting in a 3D convolutional neural network (3D CNN) [57]. This feature extraction stage yields a reduced feature vector as output, which serves as input for the classification stage, where a number of fully connected layers display a feature to partition the data into desired classes. The parameters of convolutional and fully connected layers are trained in a supervised manner. Deep learning can be applied to tumor identification in both deep fully-connected pixel-by-pixel and convolutional spatial-spectral configurations [65]. The 3D CNN model proposed in [57] consists of only two 3D layers and utilizes a limited number of training samples (20%), which are further divided into 50% for training and 50% for validation, and tested blindly (80%) on the remaining data. This study outperformed the state-of-the-art hybrid architecture, achieving an overall accuracy of 99.99%. In [51], both a classifier based on a two-dimensional convolutional neural network (2D-CNN) of three convolutional layers, one averaging pooling layer and one fully connected layer, and a deep neural network (DNN) (implemented in TensorFlow on NVIDIA Quadro K2200 GPU and trained using only spectral features of the samples) were used. Three spectral channels (λ42=591.10 nm, λ50=620.21 nm, and λ80=729.34 nm) were selected from the hypercube to highlight blood vessels in the image, the resulting images were classified using 2D-CNN. The map of parenchymatous regions was also obtained using 2D-CNN. The hypercube was fed to the 1D-DNN input, classifying the tissues in the image into four classes: normal

Таблица 2.
Методология, используемая при классификации спектрально-разрешенных изображений, регистрируемых в условиях *ex vivo*

Table 2.
Methodology used in the classification of spectrally resolved images recorded *ex vivo*

Источник Source	Подготовка материала Sample Preparation	Тип сигнала Signal type	Снижение размерности Dimensionality reduction	Методы МО ML methods
Fürtjes 2023 [66]	*ex vivo*	SRH, двухфотонная флуоресценция SRH, two-photon fluorescence		CNN
Hollon, 2021 [43]	*ex vivo*	SRH	Inception-ResNet-v2	DNN
Hollon, 2023 [42]	*ex vivo*	Stimulated Raman histology (SRH)	ResNet-50	DNN
Kast, 2015 [41]	*ex vivo*	Raman microscopy (785 nm)	(1004 $см^{-1}$), (1300–1344 $см^{-1}$), (1600 $см^{-1}$)	Многочленная логистическая модель A multinomial logistic model
Lita, 2024 [70]	FFPE	Raman microscopy (532 nm)	МГК, tSNE PCA, tSNE	KNN, DBSCAN, SVM, RF
Morais, 2019 [71]	FFPE	Raman microspectroscopy imaging (785 nm)	МГК, АПП, ГА PCA, SPA, GA	LDA, QDA, SVM
Orringer, 2017 [49]	Замороженные срезы Frozen sections	Stimulated Raman scattering (SRS) microscopy		Многослойный персептрон (MLP) Multilayer perceptron (MLP)
Uckermann, 2020 [69]	Замороженные срезы, свежий биопсийный материал Cryosections, *ex vivo* fresh biopsies	CARS, TPEF		LDA

*FFPE – фиксированные формалином и залитые парафином препараты тканей, SRH – гистология на основе вынужденного комбинационного рассеяния, МГК – метод главных компонент, АПП – алгоритм последовательных проекций, ГА – генетический алгоритм, CNN – конволюционная нейросеть, DNN – глубокая нейросеть.
*FFPE – Formalin-fixed, paraffin-embedded tissue slides, SRH – Stimulated Raman histology, PCA – Principal Component Analysis, SPA – Successive projections algorithm, CNN – convolutional neural network, DNN – deep neural network.

tissue, tumor tissue, blood vessels/hypervascularized tissue, and background. The blood vessel map was then merged with the 1D-DNN classification map by filling in the positive mask, and this result was merged with the parenchyma map using negative mask filling.

Very promising results can be obtained by combining different approaches. Moving from the works devoted to spectrally resolved imaging *in vivo* to *ex vivo* approaches, it is necessary to consider several used optical-spectral modalities at once. In [66], brain autofluorescence and neoplasia were evaluated at the microscopic level using stimulated Raman histology (SRH) combined with two-photon fluorescence. By combining two different optical effects, Raman scattering and autofluorescence with two-photon excitation, virtual images similar in structure to classical histological images obtained by hematoxylin-eosin staining with corresponding fluorescence images were obtained. Based on a previously developed convolutional neural network (CNN) based model [67], tumor, non-tumor and low quality SRH images were differentiated, and a heat map was created as an overlay on the SRH image. Using the CNN heat map, regions of interest (ROIs) were created and overlaid on the corresponding autofluorescence image to determine the average fluorescence intensity in the corresponding ROI. Another important technique for visualizing biological tissues is microscopy based on the principle of multiphoton fluorescence. The main advantage of this method of molecular imaging is high spatial resolution in combination with greater depth of penetration into the tissue, and this method shows good results even without the introduction of additional dyes, based on autofluorescence analysis [68]. Interesting results were obtained by the authors [69] using a combination of techniques such as CARS, two-photon-excited fluorescence (TPEF) and second harmonic generation on brain tumor cryosections of 382 patients and 28 healthy brain tissue samples. The texture parameters of these images were calculated and used as input for linear discriminant analysis. The combined analysis of CARS and TPEF signal texture parameters proved to be the most suitable for distinguishing between non-tumor brain tissues and brain tumors (astrocytomas of low and high malignancy, oligodendroglioma, glioblastoma, recurrent glioblastoma, and metastases) with a sensitivity of 96%, specificity of 100%. To approximate the clinical results, the results were validated on 42 fresh unfixed tumor biopsies: 82% of tumors and all non-tumor specimens were correctly identified. An image resolution of 1 μm was sufficient to distinguish between brain tumors and non-tumor brain.

The use of forced Raman microscopy with the construction of a distribution map of the ratio of protein and lipid peaks makes it possible to construct a pseudo-hematoxylin-eosin image, i.e., to use the entire accumulated histological material to classify the corresponding samples, which was brilliantly demonstrated in [42, 43].

Conclusion

Optical spectroscopy methods, due to the possibility of non-damaging interaction of light with biological tissues and wide possibilities of analyzing the content of various molecules, markers, and their structural features, are increasingly used in neurosurgery of intracranial tumors to solve the problems of intraoperative demarcation of tumor and healthy tissues. Another trend is the use of optical-spectral methods as urgent biopsy techniques. Clinical specialists are already accustomed to working with medical images, which causes their growing interest in the expansion of optical-spectral methods into the field of analyzing spectrally resolved images. However, the interpretation of such images requires a complex mathematical apparatus including both methods of preprocessing of data obtained in spatial and spectral coordinates, and methods of classification of objects and tissues in these images in order to determine the boundaries of tumor tissues during surgery, or their classification during microscopic examination. This review considers such spectrally resolved image registration methods as video fluorescence intraoperative navigation including endomicroscopy, hyperspectral intraoperative imaging in diffuse-reflected light, Raman microscopy methods. Basic machine learning methods used for tissue classification in neuro-oncology based on the analysis of such images are also presented.

This work was financially supported by the Ministry of Science and Higher Education of the Russian Federation (Agreement No. 075-15-2021-1343 dated October 4, 2021).

REFERENCES

1. Aboras M., Amasha H., Ibraheem I. Early detection of melanoma using multispectral imaging and artificial intelligence techniques, *American Journal of Biomedical and Life Sciences*, 2015, vol. 3(2–3), pp. 29–33. doi: 10.11648/j.ajbls.s.2015030203.16.
2. Kotwal A., Saragadam V., Bernstock J. D. et al. Hyperspectral imaging in neurosurgery: a review of systems, computational methods, and clinical applications, *Journal of Biomedical Optics*, 2024, vol. 30(02) doi: 10.1117/1.JBO.30.2.023512.

ЛИТЕРАТУРА

1. Aboras M., Amasha H., Ibraheem I. Early detection of melanoma using multispectral imaging and artificial intelligence techniques // American Journal of Biomedical and Life Sciences. – 2015. – Vol. 3. – № 2–3. – P. 29–33.doi: 10.11648/j.ajbls.s.2015030203.16.
2. Kotwal A., Saragadam V., Bernstock J. D. et al. Hyperspectral imaging in neurosurgery: a review of systems, computational methods, and clinical applications // Journal of Biomedical Optics. – 2024. – Vol. 30. – № 02.doi: 10.1117/1.JBO.30.2.023512.

3. Stummer W., Stocker S., Wagner S. et al. Intraoperative Detection of Malignant Gliomas by 5-Aminolevulinic Acid-induced Porphyrin Fluorescence, *Neurosurgery*, 1998, vol. 42(3), pp. 518–526. doi: 10.1097/00006123-199803000-00017.
4. Traylor J. I., Pernik M. N., Sternisha A. C. et al. Molecular and Metabolic Mechanisms Underlying Selective 5-Aminolevulinic Acid-Induced Fluorescence in Gliomas, *Cancers*, 2021, vol. 13(3), pp. 580. doi: 10.3390/cancers13030580.
5. Ivanova-Radkevich V. I., Kuznetsova O. M., Filonenko E. V. The role of membrane transport proteins in 5-ALA-induced accumulation of protoporphyrin iX in tumor cells, *Biomedical Photonics*, 2024, vol. 13(2), pp. 43–48. doi: 10.24931/2413-9432-2024-13-2-43-48.
6. Nasir-Moin M., Wadiura L. I., Sacalean V. et al. Localization of protoporphyrin IX during glioma-resection surgery via paired stimulated Raman histology and fluorescence microscopy, *Nature Biomedical Engineering*, 2024, vol. 8(6), pp. 672–688. doi: 10.1038/s41551-024-01217-3.
7. Matsumura H., Akimoto J., Haraoka J. et al. Uptake and retention of the photosensitizer mono-l-asparthyl chlorine e6 in experimental malignant glioma, *Lasers in Medical Science*, 2008, vol. 23(3), pp. 237–245. doi: 10.1007/s10103-007-0469-3.
8. Valdés P. A., Jacobs V., Harris B. T. et al. Quantitative fluorescence using 5-aminolevulinic acid-induced protoporphyrin IX biomarker as a surgical adjunct in low-grade glioma surgery, *Journal of Neurosurgery*, 2015, vol. 123(3), pp. 771–780. doi: 10.3171/2014.12.JNS14391.
9. Rynda A. Yu., Olyushin V. E., Rostovtsev D. M. et al. Results of microsurgical resection of glioblastomas under endoscopic and fluorescent control, *Biomedical Photonics*, 2024, vol. 13(3), pp. 20–30. doi: 10.24931/2413-9432-2024-13-3-20-30.
10. Goryajnov S. A., Potapov A. A., Loschenov V. B. et al. Fluorescence in neurosurgery / S. A. Goryajnov, A. A. Potapov, V. B. Loschenov et al., ed. D.Yu. Usachev, Moscow: TPS Print, 2024. (in Russ.)
11. Loshchenov M., Zelenkov P., Potapov A. et al. Endoscopic fluorescence visualization of 5-ALA photosensitized central nervous system tumors in the neural tissue transparency spectral range, *Photonics & Lasers in Medicine*, 2014, vol. 3(2) doi: 10.1515/plm-2013-0017.
12. Savelieva T. A., Loshchenov M. V., Borodkin A. V. et al. Combined spectroscopic and video fluorescent instrument for intraoperative navigation when removing a glial tumor ed. Z. Zalevsky, V. V. Tuchin, W. C. Blondel, Online Only, France: SPIE, 2020.p. 35. doi: 10.1117/12.2556064.
13. Udeneev A. M., Kalyagina N. A., Reps V. F. et al. Photo and spectral fluorescence analysis of the spinal cord injury area in animal models, *Biomedical Photonics*, 2023, vol. 12(3), pp. 15–20. doi: 10.24931/2413-9432-2023-12-3-16-20.
14. Wainwright J. V., Endo T., Cooper J. B. et al. The role of 5-aminolevulinic acid in spinal tumor surgery: a review, *Journal of Neuro-Oncology*, 2019, vol. 141(3), pp. 575–584. doi: 10.1007/s11060-018-03080-0.
15. Valdés P. A., Jacobs V. L., Leblond F. et al. Quantitative spectrally resolved intraoperative fluorescence imaging for neurosurgical guidance in brain tumor surgery: pre-clinical and clinical results ed. H. Hirschberg, S. J. Madsen, E. D. Jansen et al., San Francisco, California, United States:, 2014.p. 892809. doi: 10.1117/12.2039090.
16. Picart T., Gautheron A., Caredda C. et al. Fluorescence-Guided Surgical Techniques in Adult Diffuse Low-Grade Gliomas: State-of-the-Art and Emerging Techniques: A Systematic Review, *Cancers*, 2024, vol. 16(15), pp. 2698. doi: 10.3390/cancers16152698.
17. Maragkou T., Quint K., Pollo B. et al. Intraoperative confocal laser endomicroscopy for brain tumors - potential and challenges from a neuropathological perspective, *Free Neuropathology*, 2022, pp. 24 Pages. doi: 10.17879/FREENEUROPATHOLOGY-2022-4369.
18. Sankar T., Delaney P. M., Ryan R. W. et al. Miniaturized Handheld Confocal Microscopy for Neurosurgery: Results in an Experimental Glioblastoma Model, *Neurosurgery*, 2010, vol. 66(2), pp. 410–418. doi: 10.1227/01.NEU.0000365772.66324.6F.
19. Foersch S., Heimann A., Ayyad A. et al. Confocal Laser Endomicroscopy for Diagnosis and Histomorphologic Imaging of Brain Tumors *In Vivo*, *PLoS ONE*, 2012, vol. 7(7), pp. e41760. doi: 10.1371/journal.pone.0041760.

3. Stummer W., Stocker S., Wagner S. et al. Intraoperative Detection of Malignant Gliomas by 5-Aminolevulinic Acid-induced Porphyrin Fluorescence // Neurosurgery. – 1998. – Vol. 42. – № 3. – P. 518–526.doi: 10.1097/00006123-199803000-00017.
4. Traylor J. I., Pernik M. N., Sternisha A. C. et al. Molecular and Metabolic Mechanisms Underlying Selective 5-Aminolevulinic Acid-Induced Fluorescence in Gliomas // Cancers. – 2021. – Vol. 13. – № 3. – P. 580.doi: 10.3390/cancers13030580.
5. Ivanova-Radkevich V. I., Kuznetsova O. M., Filonenko E. V. The role of membrane transport proteins in 5-ALA-induced accumulation of protoporphyrin iX in tumor cells // Biomedical Photonics. – 2024. – Vol. 13. – № 2. – P. 43–48.doi: 10.24931/2413-9432-2024-13-2-43-48.
6. Nasir-Moin M., Wadiura L. I., Sacalean V. et al. Localization of protoporphyrin IX during glioma-resection surgery via paired stimulated Raman histology and fluorescence microscopy // Nature Biomedical Engineering. – 2024. – Vol. 8. – № 6. – P. 672–688.doi: 10.1038/s41551-024-01217-3.
7. Matsumura H., Akimoto J., Haraoka J. et al. Uptake and retention of the photosensitizer mono-l-asparthyl chlorine e6 in experimental malignant glioma // Lasers in Medical Science. – 2008. – Vol. 23. – № 3. – P. 237–245.doi: 10.1007/s10103-007-0469-3.
8. Valdés P. A., Jacobs V., Harris B. T. et al. Quantitative fluorescence using 5-aminolevulinic acid-induced protoporphyrin IX biomarker as a surgical adjunct in low-grade glioma surgery // Journal of Neurosurgery. – 2015. – Vol. 123. – № 3. – P. 771–780.doi: 10.3171/2014.12.JNS14391.
9. Rynda A. Yu., Olyushin V. E., Rostovtsev D. M. et al. Results of microsurgical resection of glioblastomas under endoscopic and fluorescent control // Biomedical Photonics. – 2024. – Vol. 13. – № 3. – P. 20–30.doi: 10.24931/2413-9432-2024-13-3-20-30.
10. Горяйнов С. А., Потапов А. А., Лощенов В. Б. и др. Флуоресценция в нейрохирургии / С. А. Горяйнов, А. А. Потапов, В. Б. Лощенов и др., под ред. Д. Ю. Усачева, Москва: ТПС Принт, 2024.
11. Loshchenov M., Zelenkov P., Potapov A. et al. Endoscopic fluorescence visualization of 5-ALA photosensitized central nervous system tumors in the neural tissue transparency spectral range // Photonics & Lasers in Medicine. – 2014. – Vol. 3. – № 2.doi: 10.1515/plm-2013-0017.
12. Savelieva T. A., Loshchenov M. V., Borodkin A. V. et al. Combined spectroscopic and video fluorescent instrument for intraoperative navigation when removing a glial tumor ed. Z. Zalevsky, V. V. Tuchin, W. C. Blondel, Online Only, France: SPIE, 2020. C. 35.doi: 10.1117/12.2556064.
13. Udeneev A. M., Kalyagina N. A., Reps V. F. et al. Photo and spectral fluorescence analysis of the spinal cord injury area in animal models // Biomedical Photonics. – 2023. – Vol. 12. – № 3. – P. 15–20. doi: 10.24931/2413-9432-2023-12-3-16-20.
14. Wainwright J. V., Endo T., Cooper J. B. et al. The role of 5-aminolevulinic acid in spinal tumor surgery: a review // Journal of Neuro-Oncology. – 2019. – Vol. 141. – № 3. – P. 575–584.doi: 10.1007/s11060-018-03080-0.
15. Valdés P. A., Jacobs V. L., Leblond F. et al. Quantitative spectrally resolved intraoperative fluorescence imaging for neurosurgical guidance in brain tumor surgery: pre-clinical and clinical results ed. H. Hirschberg, S. J. Madsen, E. D. Jansen et al., San Francisco, California, United States, 2014. C. 892809.doi: 10.1117/12.2039090.
16. Picart T., Gautheron A., Caredda C. et al. Fluorescence-Guided Surgical Techniques in Adult Diffuse Low-Grade Gliomas: State-of-the-Art and Emerging Techniques: A Systematic Review // Cancers. – 2024. – Vol. 16. – № 15. – P. 2698.doi: 10.3390/cancers16152698.
17. Maragkou T., Quint K., Pollo B. et al. Intraoperative confocal laser endomicroscopy for brain tumors - potential and challenges from a neuropathological perspective // Free Neuropathology. – 2022. – P. 24 Pages.doi: 10.17879/FREENEUROPATHOLOGY-2022-4369.
18. Sankar T., Delaney P. M., Ryan R. W. et al. Miniaturized Handheld Confocal Microscopy for Neurosurgery: Results in an Experimental Glioblastoma Model // Neurosurgery. – 2010. – Vol. 66. – № 2. – P. 410–418.doi: 10.1227/01.NEU.0000365772.66324.6F.
19. Foersch S., Heimann A., Ayyad A. et al. Confocal Laser Endomicroscopy for Diagnosis and Histomorphologic Imaging of Brain Tumors *In Vivo* // PLoS ONE. – 2012. – Vol. 7. – № 7. – P. e41760.doi: 10.1371/journal.pone.0041760.

20. Martirosyan N. L., Cavalcanti D. D., Eschbacher J. M. et al. Use of *in vivo* near-infrared laser confocal endomicroscopy with indocyanine green to detect the boundary of infiltrative tumor: Laboratory investigation, *Journal of Neurosurgery*, 2011, vol. 115(6), pp. 1131–1138. doi: 10.3171/2011.8.JNS11559.
21. Sanai N., Eschbacher J., Hattendorf G. et al. Intraoperative Confocal Microscopy for Brain Tumors: A Feasibility Analysis in Humans, *Operative Neurosurgery*, 2011, vol. 68, pp. ons282–ons290. doi: 10.1227/NEU.0b013e318212464e.
22. Sanai N., Snyder L. A., Honea N. J. et al. Intraoperative confocal microscopy in the visualization of 5-aminolevulinic acid fluorescence in low-grade gliomas: Clinical article, *Journal of Neurosurgery*, 2011, vol. 115(4), pp. 740–748. doi: 10.3171/2011.6.JNS11252.
23. Eschbacher J., Martirosyan N. L., Nakaji P. et al. *In vivo* intraoperative confocal microscopy for real-time histopathological imaging of brain tumors: Clinical article, *Journal of Neurosurgery*, 2012, vol. 116(4), pp. 854–860. doi: 10.3171/2011.12.JNS11696.
24. Pavlov V., Meyronet D., Meyer-Bisch V. et al. Intraoperative Probe-Based Confocal Laser Endomicroscopy in Surgery and Stereotactic Biopsy of Low-Grade and High-Grade Gliomas: A Feasibility Study in Humans, *Neurosurgery*, 2016, vol. 79(4), pp. 604–612. doi: 10.1227/NEU.0000000000001365.
25. Liu J. T. C., Meza D., Sanai N. Trends in Fluorescence Image-Guided Surgery for Gliomas, *Neurosurgery*, 2014, vol. 75(1), pp. 61–71. doi: 10.1227/NEU.0000000000000344.
26. Sibai M., Veilleux I., Elliott J. T. et al. Quantitative spatial frequency fluorescence imaging in the sub-diffusive domain for image-guided glioma resection, *Biomedical Optics Express*, 2015, vol. 6(12), pp. 4923. doi: 10.1364/BOE.6.004923.
27. Wirth D., Kolste K., Kanick S. et al. Fluorescence depth estimation from wide-field optical imaging data for guiding brain tumor resection: a multi-inclusion phantom study, *Biomedical Optics Express*, 2017, vol. 8(8), pp. 3656. doi: 10.1364/BOE.8.003656.
28. Belykh E., Miller E. J., Carotenuto A. et al. Progress in Confocal Laser Endomicroscopy for Neurosurgery and Technical Nuances for Brain Tumor Imaging With Fluorescein, *Frontiers in Oncology*, 2019, vol. 9, pp. 554. doi: 10.3389/fonc.2019.00554.
29. Abramov I., Park M. T., Belykh E. et al. Intraoperative confocal laser endomicroscopy: prospective *in vivo* feasibility study of a clinical-grade system for brain tumors, *Journal of Neurosurgery*, 2023, vol. 138(3), pp. 587–597. doi: 10.3171/2022.5.JNS2282.
30. Belykh E., Miller E. J., Patel A. A. et al. Diagnostic Accuracy of a Confocal Laser Endomicroscope for *In Vivo* Differentiation Between Normal Injured And Tumor Tissue During Fluorescein-Guided Glioma Resection: Laboratory Investigation, *World Neurosurgery*, 2018, vol. 115, pp. e337–e348. doi: 10.1016/j.wneu.2018.04.048.
31. Acerbi F., Pollo B., De Laurentis C. et al. *Ex Vivo* Fluorescein-Assisted Confocal Laser Endomicroscopy (CONVIVO® System) in Patients With Glioblastoma: Results From a Prospective Study, *Frontiers in Oncology*, 2020, vol. 10, pp. 606574. doi: 10.3389/fonc.2020.606574.
32. Giannoni L., Bonaudo C., Marradi M. et al. Optical characterisation and study of *ex vivo* glioma tissue for hyperspectral imaging during neurosurgery ed. D. Contini, Y. Hoshi, T. D. O'Sullivan, Munich, Germany: SPIE, 2023.p. 81. doi: 10.1117/12.2670854.
33. Fabelo H., Ortega S., Kabwama S. et al. HELICoiD project: a new use of hyperspectral imaging for brain cancer detection in real-time during neurosurgical operations ed. D. P. Bannon, Baltimore, Maryland, United States:, 2016.p. 986002. doi: 10.1117/12.2223075.
34. Fabelo H., Ortega S., Lazcano R. et al. An Intraoperative Visualization System Using Hyperspectral Imaging to Aid in Brain Tumor Delineation, *Sensors*, 2018, vol. 18(2), pp. 430. doi: 10.3390/s18020430.
35. Ezhov I., Giannoni L., Shit S. et al. Identifying chromophore fingerprints of brain tumor tissue on hyperspectral imaging using principal component analysis ed. D. Contini, Y. Hoshi, T. D. O'Sullivan, Munich, Germany: SPIE, 2023.p. 78. doi: 10.1117/12.2670775.
36. Martinez B., Leon R., Fabelo H. et al. Most Relevant Spectral Bands Identification for Brain Cancer Detection Using Hyperspectral Imaging, *Sensors*, 2019, vol. 19(24), pp. 5481. doi: 10.3390/s19245481.

20. Martirosyan N. L., Cavalcanti D. D., Eschbacher J. M. et al. Use of *in vivo* near-infrared laser confocal endomicroscopy with indocyanine green to detect the boundary of infiltrative tumor: Laboratory investigation // Journal of Neurosurgery. – 2011. – Vol. 115. – № 6. – P. 1131–1138.doi: 10.3171/2011.8.JNS11559.
21. Sanai N., Eschbacher J., Hattendorf G. et al. Intraoperative Confocal Microscopy for Brain Tumors: A Feasibility Analysis in Humans // Operative Neurosurgery. – 2011. – Vol. 68. – P. ons282–ons290.doi: 10.1227/NEU.0b013e318212464e.
22. Sanai N., Snyder L. A., Honea N. J. et al. Intraoperative confocal microscopy in the visualization of 5-aminolevulinic acid fluorescence in low-grade gliomas: Clinical article // Journal of Neurosurgery. – 2011. – Vol. 115. – № 4. – P. 740–748.doi: 10.3171/2011.6.JNS11252.
23. Eschbacher J., Martirosyan N. L., Nakaji P. et al. *In vivo* intraoperative confocal microscopy for real-time histopathological imaging of brain tumors: Clinical article // Journal of Neurosurgery. – 2012. – Vol. 116. – № 4. – P. 854–860.doi: 10.3171/2011.12.JNS11696.
24. Pavlov V., Meyronet D., Meyer-Bisch V. et al. Intraoperative Probe-Based Confocal Laser Endomicroscopy in Surgery and Stereotactic Biopsy of Low-Grade and High-Grade Gliomas: A Feasibility Study in Humans // Neurosurgery. – 2016. – Vol. 79. – № 4. – P. 604–612. doi: 10.1227/NEU.0000000000001365.
25. Liu J. T. C., Meza D., Sanai N. Trends in Fluorescence Image-Guided Surgery for Gliomas // Neurosurgery. – 2014. – Vol. 75. – № 1. – P. 61–71.doi: 10.1227/NEU.0000000000000344.
26. Sibai M., Veilleux I., Elliott J. T. et al. Quantitative spatial frequency fluorescence imaging in the sub-diffusive domain for image-guided glioma resection // Biomedical Optics Express. – 2015. – Vol. 6. – № 12. – P. 4923.doi: 10.1364/BOE.6.004923.
27. Wirth D., Kolste K., Kanick S. et al. Fluorescence depth estimation from wide-field optical imaging data for guiding brain tumor resection: a multi-inclusion phantom study // Biomedical Optics Express. – 2017. – Vol. 8. – № 8. – P. 3656.doi: 10.1364/BOE.8.003656.
28. Belykh E., Miller E. J., Carotenuto A. et al. Progress in Confocal Laser Endomicroscopy for Neurosurgery and Technical Nuances for Brain Tumor Imaging With Fluorescein // Frontiers in Oncology. – 2019. – Vol. 9. – P. 554.doi: 10.3389/fonc.2019.00554.
29. Abramov I., Park M. T., Belykh E. et al. Intraoperative confocal laser endomicroscopy: prospective *in vivo* feasibility study of a clinical-grade system for brain tumors // Journal of Neurosurgery. – 2023. – Vol. 138. – № 3. – P. 587–597.doi: 10.3171/2022.5.JNS2282.
30. Belykh E., Miller E. J., Patel A. A. et al. Diagnostic Accuracy of a Confocal Laser Endomicroscope for *In Vivo* Differentiation Between Normal Injured And Tumor Tissue During Fluorescein-Guided Glioma Resection: Laboratory Investigation // World Neurosurgery. – 2018. – Vol. 115. – P. e337–e348.doi: 10.1016/j.wneu.2018.04.048.
31. Acerbi F., Pollo B., De Laurentis C. et al. *Ex Vivo* Fluorescein-Assisted Confocal Laser Endomicroscopy (CONVIVO® System) in Patients With Glioblastoma: Results From a Prospective Study // Frontiers in Oncology. – 2020. – Vol. 10. – P. 606574.doi: 10.3389/fonc.2020.606574.
32. Giannoni L., Bonaudo C., Marradi M. et al. Optical characterisation and study of *ex vivo* glioma tissue for hyperspectral imaging during neurosurgery ed. D. Contini, Y. Hoshi, T. D. O'Sullivan, Munich, Germany: SPIE, 2023. C. 81.doi: 10.1117/12.2670854.
33. Fabelo H., Ortega S., Kabwama S. et al. HELICoiD project: a new use of hyperspectral imaging for brain cancer detection in real-time during neurosurgical operations ed. D. P. Bannon, Baltimore, Maryland, United States:, 2016. C. 986002.doi: 10.1117/12.2223075.
34. Fabelo H., Ortega S., Lazcano R. et al. An Intraoperative Visualization System Using Hyperspectral Imaging to Aid in Brain Tumor Delineation // Sensors. – 2018. – Vol. 18. – № 2. – P. 430.doi: 10.3390/s18020430.
35. Ezhov I., Giannoni L., Shit S. et al. Identifying chromophore fingerprints of brain tumor tissue on hyperspectral imaging using principal component analysis ed. D. Contini, Y. Hoshi, T. D. O'Sullivan, Munich, Germany: SPIE, 2023. C. 78.doi: 10.1117/12.2670775.
36. Martinez B., Leon R., Fabelo H. et al. Most Relevant Spectral Bands Identification for Brain Cancer Detection Using Hyperspectral Imaging // Sensors. – 2019. – Vol. 19. – № 24. – P. 5481.doi: 10.3390/s19245481.

37. DePaoli D., Lemoine É., Ember K. et al. Rise of Raman spectroscopy in neurosurgery: a review, *Journal of Biomedical Optics*, 2020, vol. 25(05), pp. 1. doi: 10.1117/1.JBO.25.5.050901.
38. Romanishkin I. D., Savelieva T. A., Ospanov A. et al. Classification of intracranial tumors based on optical-spectral analysis, *Biomedical Photonics*, 2023, vol. 12(3), pp. 4–10. doi: 10.24931/2413-9432-2023-12-3-4-10.
39. Romanishkin I., Savelieva T., Kosyrkova A. et al. Differentiation of glioblastoma tissues using spontaneous Raman scattering with dimensionality reduction and data classification, *Frontiers in Oncology*, 2022, vol. 12, pp. 944210. doi: 10.3389/fonc.2022.944210.
40. Hollon T., Orringer D. A. Label-free brain tumor imaging using Raman-based methods, *Journal of Neuro-Oncology*, 2021, vol. 151(3), pp. 393–402. doi: 10.1007/s11060-019-03380-z.
41. Kast R., Auner G., Yurgelevic S. et al. Identification of regions of normal grey matter and white matter from pathologic glioblastoma and necrosis in frozen sections using Raman imaging, *Journal of Neuro-Oncology*, 2015, vol. 125(2), pp. 287–295. doi: 10.1007/s11060-015-1929-4.
42. Hollon T., Jiang C., Chowdury A. et al. Artificial-intelligence-based molecular classification of diffuse gliomas using rapid, label-free optical imaging, *Nature Medicine*, 2023, vol. 29(4), pp. 828–832. doi: 10.1038/s41591-023-02252-4.
43. Hollon T. C., Pandian B., Adapa A. R. et al. Near real-time intraoperative brain tumor diagnosis using stimulated Raman histology and deep neural networks, *Nature Medicine*, 2020, vol. 26(1), pp. 52–58. doi: 10.1038/s41591-019-0715-9.
44. Evans C. L., Xu X., Kesari S. et al. Chemically-selective imaging of brain structures with CARS microscopy, *Optics Express*, 2007, vol. 15(19), pp. 12076. doi: 10.1364/OE.15.012076.
45. Uckermann O., Galli R., Tamosaityte S. et al. Label-Free Delineation of Brain Tumors by Coherent Anti-Stokes Raman Scattering Microscopy in an Orthotopic Mouse Model and Human Glioblastoma, *PLoS ONE*, 2014, vol. 9(9), pp. e107115. doi: 10.1371/journal.pone.0107115.
46. Mascagni P., Alapatt D., Sestini L. et al. Computer vision in surgery: from potential to clinical value, *npj Digital Medicine*, 2022, vol. 5(1), pp. 163. doi: 10.1038/s41746-022-00707-5.
47. Rau A., Edwards P. J. E., Ahmad O. F. et al. Implicit domain adaptation with conditional generative adversarial networks for depth prediction in endoscopy, *International Journal of Computer Assisted Radiology and Surgery*, 2019, vol. 14(7), pp. 1167–1176. doi: 10.1007/s11548-019-01962-w.
48. Kassem H., Alapatt D., Mascagni P. et al. Federated Cycling (FedCy): Semi-Supervised Federated Learning of Surgical Phases, *IEEE Transactions on Medical Imaging*, 2023, vol. 42(7), pp. 1920–1931. doi: 10.1109/TMI.2022.3222126.
49. Orringer D. A., Pandian B., Niknafs Y. S. et al. Rapid intraoperative histology of unprocessed surgical specimens via fibre-laser-based stimulated Raman scattering microscopy, *Nature Biomedical Engineering*, 2017, vol. 1(2), pp. 0027. doi: 10.1038/s41551-016-0027.
50. Leon R., Fabelo H., Ortega S. et al. Hyperspectral imaging benchmark based on machine learning for intraoperative brain tumour detection, *npj Precision Oncology*, 2023, vol. 7(1), pp. 119. doi: 10.1038/s41698-023-00475-9.
51. Fabelo H., Halicek M., Ortega S. et al. Deep Learning-Based Framework for *In Vivo* Identification of Glioblastoma Tumor using Hyperspectral Images of Human Brain, *Sensors*, 2019, vol. 19(4), pp. 920. doi: 10.3390/s19040920.
52. Ravi D., Fabelo H., Callic G. M. et al. Manifold Embedding and Semantic Segmentation for Intraoperative Guidance With Hyperspectral Brain Imaging, *IEEE Transactions on Medical Imaging*, 2017, vol. 36(9), pp. 1845–1857. doi: 10.1109/TMI.2017.2695523.
53. Fabelo H., Ortega S., Ravi D. et al. Spatio-spectral classification of hyperspectral images for brain cancer detection during surgical operations, *PLOS ONE*, 2018, vol. 13(3), pp. e0193721. doi: 10.1371/journal.pone.0193721.
54. Florimbi G., Fabelo H., Torti E. et al. Accelerating the K-Nearest Neighbors Filtering Algorithm to Optimize the Real-Time Classification of Human Brain Tumor in Hyperspectral Images, *Sensors*, 2018, vol. 18(7), pp. 2314. doi: 10.3390/s18072314.

37. DePaoli D., Lemoine É., Ember K. et al. Rise of Raman spectroscopy in neurosurgery: a review // Journal of Biomedical Optics. – 2020. – Vol. 25. – № 05. – P. 1.doi: 10.1117/1.JBO.25.5.050901.
38. Romanishkin I. D., Savelieva T. A., Ospanov A. et al. Classification of intracranial tumors based on optical-spectral analysis // Biomedical Photonics. – 2023. – Vol. 12. – № 3. – P. 4–10.doi: 10.24931/2413-9432-2023-12-3-4-10.
39. Romanishkin I., Savelieva T., Kosyrkova A. et al. Differentiation of glioblastoma tissues using spontaneous Raman scattering with dimensionality reduction and data classification // Frontiers in Oncology. – 2022. – Vol. 12. – P. 944210.doi: 10.3389/fonc.2022.944210.
40. Hollon T., Orringer D. A. Label-free brain tumor imaging using Raman-based methods // Journal of Neuro-Oncology. – 2021. – Vol. 151. – № 3. – P. 393–402.doi: 10.1007/s11060-019-03380-z.
41. Kast R., Auner G., Yurgelevic S. et al. Identification of regions of normal grey matter and white matter from pathologic glioblastoma and necrosis in frozen sections using Raman imaging // Journal of Neuro-Oncology. – 2015. – Vol. 125. – № 2. – P. 287–295.doi: 10.1007/s11060-015-1929-4.
42. Hollon T., Jiang C., Chowdury A. et al. Artificial-intelligence-based molecular classification of diffuse gliomas using rapid, label-free optical imaging // Nature Medicine. – 2023. – Vol. 29. – № 4. – P. 828–832.doi: 10.1038/s41591-023-02252-4.
43. Hollon T. C., Pandian B., Adapa A. R. et al. Near real-time intraoperative brain tumor diagnosis using stimulated Raman histology and deep neural networks // Nature Medicine. – 2020. – Vol. 26. – № 1. – P. 52–58.doi: 10.1038/s41591-019-0715-9.
44. Evans C. L., Xu X., Kesari S. et al. Chemically-selective imaging of brain structures with CARS microscopy // Optics Express. – 2007. – Vol. 15. – № 19. – P. 12076.doi: 10.1364/OE.15.012076.
45. Uckermann O., Galli R., Tamosaityte S. et al. Label-Free Delineation of Brain Tumors by Coherent Anti-Stokes Raman Scattering Microscopy in an Orthotopic Mouse Model and Human Glioblastoma // PLoS ONE. – 2014. – Vol. 9. – № 9. – P. e107115.doi: 10.1371/journal.pone.0107115.
46. Mascagni P., Alapatt D., Sestini L. et al. Computer vision in surgery: from potential to clinical value // npj Digital Medicine. – 2022. – Vol. 5. – № 1. – P. 163.doi: 10.1038/s41746-022-00707-5.
47. Rau A., Edwards P. J. E., Ahmad O. F. et al. Implicit domain adaptation with conditional generative adversarial networks for depth prediction in endoscopy // International Journal of Computer Assisted Radiology and Surgery. – 2019. – Vol. 14. – № 7. – P. 1167–1176.doi: 10.1007/s11548-019-01962-w.
48. Kassem H., Alapatt D., Mascagni P. et al. Federated Cycling (FedCy): Semi-Supervised Federated Learning of Surgical Phases // IEEE Transactions on Medical Imaging. – 2023. – Vol. 42. – № 7. – P. 1920–1931.doi: 10.1109/TMI.2022.3222126.
49. Orringer D. A., Pandian B., Niknafs Y. S. et al. Rapid intraoperative histology of unprocessed surgical specimens via fibre-laser-based stimulated Raman scattering microscopy // Nature Biomedical Engineering. – 2017. – Vol. 1. – № 2. – P. 0027.doi: 10.1038/s41551-016-0027.
50. Leon R., Fabelo H., Ortega S. et al. Hyperspectral imaging benchmark based on machine learning for intraoperative brain tumour detection // npj Precision Oncology. – 2023. – Vol. 7. – № 1. – P. 119.doi: 10.1038/s41698-023-00475-9.
51. Fabelo H., Halicek M., Ortega S. et al. Deep Learning-Based Framework for *In Vivo* Identification of Glioblastoma Tumor using Hyperspectral Images of Human Brain // Sensors. – 2019. – Vol. 19. – № 4. – P. 920.doi: 10.3390/s19040920.
52. Ravi D., Fabelo H., Callic G. M. et al. Manifold Embedding and Semantic Segmentation for Intraoperative Guidance With Hyperspectral Brain Imaging // IEEE Transactions on Medical Imaging. – 2017. – Vol. 36. – № 9. – P. 1845–1857.doi: 10.1109/TMI.2017.2695523.
53. Fabelo H., Ortega S., Ravi D. et al. Spatio-spectral classification of hyperspectral images for brain cancer detection during surgical operations // PLOS ONE. – 2018. – Vol. 13. – № 3. – P. e0193721.doi: 10.1371/journal.pone.0193721.
54. Florimbi G., Fabelo H., Torti E. et al. Accelerating the K-Nearest Neighbors Filtering Algorithm to Optimize the Real-Time Classification of Human Brain Tumor in Hyperspectral Images // Sensors. – 2018. – Vol. 18. – № 7. – P. 2314.doi: 10.3390/s18072314.

55. Zhang Y., Cao G., Li X. et al. Cascaded Random Forest for Hyperspectral Image Classification, *IEEE Journal of Selected Topics in Applied Earth Observations and Remote Sensing*, 2018, vol. 11(4), pp. 1082–1094. doi: 10.1109/JSTARS.2018.2809781.
56. Xia J., Ghamisi P., Yokoya N. et al. Random Forest Ensembles and Extended Multiextinction Profiles for Hyperspectral Image Classification, *IEEE Transactions on Geoscience and Remote Sensing*, 2018, vol. 56(1), pp. 202–216. doi: 10.1109/TGRS.2017.2744662.
57. Ayaz H., Tormey D., McLoughlin I. et al. Hyperspectral Brain Tissue Classification using a Fast and Compact 3D CNN Approach Genova, Italy: IEEE, 2022.p. 1–4. doi: 10.1109/IPAS55744.2022.10053044.
58. Baig N., Fabelo H., Ortega S. et al. Empirical Mode Decomposition Based Hyperspectral Data Analysis for Brain Tumor Classification Mexico: IEEE, 2021.p. 2274–2277. doi: 10.1109/EMBC46164.2021.9629676.
59. Cruz-Guerrero I. A., Leon R., Campos-Delgado D. U. et al. Classification of Hyperspectral *In Vivo* Brain Tissue Based on Linear Unmixing, *Applied Sciences*, 2020, vol. 10(16), pp. 5686. doi: 10.3390/app10165686.
60. Ruiz L., Martin A., Urbanos G. et al. Multiclass Brain Tumor Classification Using Hyperspectral Imaging and Supervised Machine Learning Segovia, Spain: IEEE, 2020.p. 1–6. doi: 10.1109/DCIS51330.2020.9268650.
61. Salvador R., Fabelo H., Lazcano R. et al. Demo: HELICoiD tool demonstrator for real-time brain cancer detection Rennes, France: IEEE, 2016.p. 237–238. doi: 10.1109/DASIP.2016.7853831.
62. Sutradhar P., Sancho J., Villa M. et al. Exploration of Realtime Brain tumor classification from Hyperspectral Images in Heterogeneous Embedded MPSoC Pamplona, Spain: IEEE, 2022.p. 01–06. doi: 10.1109/DCIS55711.2022.9970064.
63. Torti E., Florimbi G., Castelli F. et al. Parallel K-Means Clustering for Brain Cancer Detection Using Hyperspectral Images, *Electronics*, 2018, vol. 7(11), pp. 283. doi: 10.3390/electronics7110283.
64. Urbanos G., Martín A., Vázquez G. et al. Supervised Machine Learning Methods and Hyperspectral Imaging Techniques Jointly Applied for Brain Cancer Classification, *Sensors*, 2021, vol. 21(11), pp. 3827. doi: 10.3390/s21113827.
65. Manni F., Van Der Sommen F., Fabelo H. et al. Hyperspectral Imaging for Glioblastoma Surgery: Improving Tumor Identification Using a Deep Spectral-Spatial Approach, *Sensors*, 2020, vol. 20(23), pp. 6955. doi: 10.3390/s20236955.
66. Fürtjes G., Reinecke D., Von Spreckelsen N. et al. Intraoperative microscopic autofluorescence detection and characterization in brain tumors using stimulated Raman histology and two-photon fluorescence, *Frontiers in Oncology*, 2023, vol. 13, pp. 1146031. doi: 10.3389/fonc.2023.1146031.
67. Reinecke D., Von Spreckelsen N., Mawrin C. et al. Novel rapid intraoperative qualitative tumor detection by a residual convolutional neural network using label-free stimulated Raman scattering microscopy, *Acta Neuropathologica Communications*, 2022, vol. 10(1), pp. 109. doi: 10.1186/s40478-022-01411-x.
68. Shirshin E. A., Yakimov B. P., Darvin M. E. et al. Label-Free Multiphoton Microscopy: The Origin of Fluorophores and Capabilities for Analyzing Biochemical Processes, *Biochemistry (Moscow)*, 2019, vol. 84(S1), pp. 69–88. doi: 10.1134/S0006297919140050.
69. Uckermann O., Galli R., Mark G. et al. Label-free multiphoton imaging allows brain tumor recognition based on texture analysis–a study of 382 tumor patients, *Neuro-Oncology Advances*, 2020, vol. 2(1), pp. vdaa035. doi: 10.1093/noajnl/vdaa035.
70. Lita A., Sjöberg J., Păcioianu D. et al. Raman-based machine-learning platform reveals unique metabolic differences between IDHmut and IDHwt glioma, *Neuro-Oncology*, 2024, vol. 26(11), pp. 1994–2009. doi: 10.1093/neuonc/noae101.
71. Morais C. L. M., Lilo T., Ashton K. M. et al. Determination of meningioma brain tumour grades using Raman micro-spectroscopy imaging, *The Analyst*, 2019, vol. 144(23), pp. 7024–7031. doi: 10.1039/C9AN01551E.

55. Zhang Y., Cao G., Li X. et al. Cascaded Random Forest for Hyperspectral Image Classification // IEEE Journal of Selected Topics in Applied Earth Observations and Remote Sensing. – 2018. – Vol. 11. – № 4. – P. 1082–1094.doi: 10.1109/JSTARS.2018.2809781.
56. Xia J., Ghamisi P., Yokoya N. et al. Random Forest Ensembles and Extended Multiextinction Profiles for Hyperspectral Image Classification // IEEE Transactions on Geoscience and Remote Sensing. – 2018. – Vol. 56. – № 1. – P. 202–216.doi: 10.1109/TGRS.2017.2744662.
57. Ayaz H., Tormey D., McLoughlin I. et al. Hyperspectral Brain Tissue Classification using a Fast and Compact 3D CNN Approach Genova, Italy: IEEE, 2022. C. 1–4.doi: 10.1109/IPAS55744.2022.10053044.
58. Baig N., Fabelo H., Ortega S. et al. Empirical Mode Decomposition Based Hyperspectral Data Analysis for Brain Tumor Classification Mexico: IEEE, 2021. C. 2274–2277.doi: 10.1109/EMBC46164.2021.9629676.
59. Cruz-Guerrero I. A., Leon R., Campos-Delgado D. U. et al. Classification of Hyperspectral *In Vivo* Brain Tissue Based on Linear Unmixing // Applied Sciences. – 2020. – Vol. 10. – № 16. – P. 5686. doi: 10.3390/app10165686.
60. Ruiz L., Martin A., Urbanos G. et al. Multiclass Brain Tumor Classification Using Hyperspectral Imaging and Supervised Machine Learning Segovia, Spain: IEEE, 2020. C. 1–6.doi: 10.1109/DCIS51330.2020.9268650.
61. Salvador R., Fabelo H., Lazcano R. et al. Demo: HELICoiD tool demonstrator for real-time brain cancer detection Rennes, France: IEEE, 2016. C. 237–238.doi: 10.1109/DASIP.2016.7853831.
62. Sutradhar P., Sancho J., Villa M. et al. Exploration of Realtime Brain tumor classification from Hyperspectral Images in Heterogeneous Embedded MPSoC Pamplona, Spain: IEEE, 2022. C. 01–06.doi: 10.1109/DCIS55711.2022.9970064.
63. Torti E., Florimbi G., Castelli F. et al. Parallel K-Means Clustering for Brain Cancer Detection Using Hyperspectral Images // Electronics. – 2018. – Vol. 7. – № 11. – P. 283.doi: 10.3390/electronics7110283.
64. Urbanos G., Martín A., Vázquez G. et al. Supervised Machine Learning Methods and Hyperspectral Imaging Techniques Jointly Applied for Brain Cancer Classification // Sensors. – 2021. – Vol. 21. – № 11. – P. 3827.doi: 10.3390/s21113827.
65. Manni F., Van Der Sommen F., Fabelo H. et al. Hyperspectral Imaging for Glioblastoma Surgery: Improving Tumor Identification Using a Deep Spectral-Spatial Approach // Sensors. – 2020. – Vol. 20. – № 23. – P. 6955.doi: 10.3390/s20236955.
66. Fürtjes G., Reinecke D., Von Spreckelsen N. et al. Intraoperative microscopic autofluorescence detection and characterization in brain tumors using stimulated Raman histology and two-photon fluorescence // Frontiers in Oncology. – 2023. – Vol. 13. – P. 1146031.doi: 10.3389/fonc.2023.1146031.
67. Reinecke D., Von Spreckelsen N., Mawrin C. et al. Novel rapid intraoperative qualitative tumor detection by a residual convolutional neural network using label-free stimulated Raman scattering microscopy // Acta Neuropathologica Communications. – 2022. – Vol. 10. – № 1. – P. 109.doi: 10.1186/s40478-022-01411-x.
68. Shirshin E. A., Yakimov B. P., Darvin M. E. et al. Label-Free Multiphoton Microscopy: The Origin of Fluorophores and Capabilities for Analyzing Biochemical Processes // Biochemistry (Moscow). – 2019. – Vol. 84. – № S1. – P. 69–88.doi: 10.1134/S0006297919140050.
69. Uckermann O., Galli R., Mark G. et al. Label-free multiphoton imaging allows brain tumor recognition based on texture analysis—a study of 382 tumor patients // Neuro-Oncology Advances. – 2020. – Vol. 2. – № 1. – P. vdaa035.doi: 10.1093/noajnl/vdaa035.
70. Lita A., Sjöberg J., Păcioianu D. et al. Raman-based machine-learning platform reveals unique metabolic differences between IDHmut and IDHwt glioma // Neuro-Oncology. – 2024. – Vol. 26. – № 11. – P. 1994–2009.doi: 10.1093/neuonc/noae101.
71. Morais C. L. M., Lilo T., Ashton K. M. et al. Determination of meningioma brain tumour grades using Raman microspectroscopy imaging // The Analyst. – 2019. – Vol. 144. – № 23. – P. 7024–7031. doi: 10.1039/C9AN01551E.